ACS EARTH AND SPACE CHEMISTRY

http://pubs.acs.org/journal/aesccq
Article

Leaf-Level Bidirectional Exchange of Formaldehyde on Deciduous and Evergreen Tree Saplings

Joshua D. Shutter,[⊥] Joshua L. Cox,[⊥] and Frank N. Keutsch*

Cite This: ACS Earth Space Chem. 2024, 8, 723−733
Read Online

ACCESS | Metrics & More | Article Recommendations | Supporting Information

ABSTRACT: Gas-phase formaldehyde (HCHO) is formed in high yield from the oxidation of many volatile organic compounds (VOCs) and is commonly used as a constraint when testing the performance of VOC oxidation mechanisms in models. However, prior to using HCHO as a model constraint for VOC oxidation in forested regions, it is essential to have a thorough understanding of its foliar exchange. Therefore, a controlled laboratory setup was designed to measure the emission and dry deposition of HCHO at the leaf-level to red oak (*Quercus rubra*) and Leyland cypress (*Cupressus* × *leylandii*) tree saplings. The results show that HCHO has a compensation point (CP) that rises exponentially with temperature (22−35 °C) with a mean range of 0.3−0.9 ppbv. The HCHO CP results are also found to be independent of the studied tree species and 40−70% relative humidity. Given that HCHO mixing ratios in forests during the daytime are usually greater than 1 ppbv, the magnitude of the CP suggests that trees generally act as a net sink of HCHO. Additionally, the results show that HCHO foliar exchange is stomatally controlled and better matches a reactivity factor (f_0) of 0 as opposed to 1 in conventional dry deposition parametrizations. At 30 °C, daytime HCHO dry deposition fluxes are reduced by upward of 50% when using $f_0 = 0$ and a nonzero HCHO CP, although deposition remains the dominant canopy sink of HCHO. A reduced deposition sink also implies the increased importance of the gas-phase photolysis of HCHO as a source of HO_2.

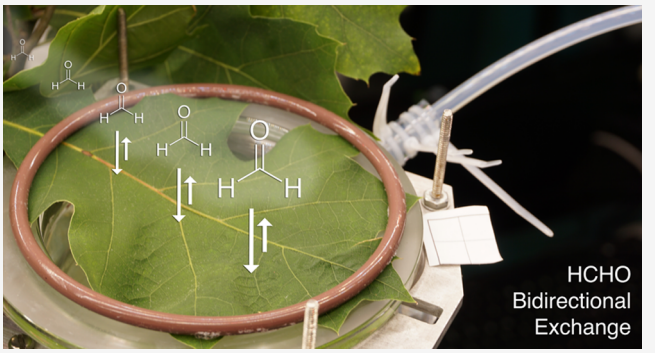

KEYWORDS: *formaldehyde, bidirectional exchange, dry deposition, compensation point, stomatal uptake, trees*

1. INTRODUCTION

The biosphere plays a key role in the chemical composition of the atmosphere since it acts as a large source and sink of reactive organic carbon.[1] As a source, biogenic emissions of volatile organic compounds (VOCs) are estimated to be around 1000 Tg yr^{-1}, and the oxidation of these VOCs impacts the climate system and human health as it is coupled to the production of tropospheric ozone (O_3) and secondary organic aerosol (SOA).[2] The biosphere also acts as an important sink of oxygenated VOCs (i.e., OVOCs) via dry deposition.[3] For example, Knote et al. have shown that including dry deposition of OVOCs in a regional chemistry transport model (WRF-Chem) reduced SOA by nearly 50% over the continental U.S. in 2010.[4] While dry deposition clearly plays a significant role in affecting atmospheric composition and the lifetime of chemical species, there also exists a lack of experimental data to constrain the deposition sink for many compounds.[3,5−7]

One such OVOC lacking a robust constraint on deposition is formaldehyde (HCHO).[8] As a ubiquitous byproduct from the oxidation of VOCs, the measurement of HCHO both *in situ* and via satellite has been used extensively to constrain VOC emissions from both biogenic and anthropogenic sources and to test understanding of VOC oxidation chemistry mechanisms in models.[9−14] However, to successfully use HCHO as an oxidative tracer, it is crucial to determine the magnitude of its sources and sinks. With an atmospheric lifetime of around several hours during the day, its mixing ratio reflects recent oxidation. Alongside deposition, additional sinks of HCHO include loss by OH and photolysis, both of which can contribute significantly as a source of HO_x (HO_x = OH + HO_2) radicals to the atmosphere.[15,16]

It is also known that HCHO can be emitted directly from foliage.[17−23] OVOCs like HCHO that can be emitted from leaves exhibit bidirectional exchange since their exchange with leaves depends on (1) the concentration gradient between the intercellular air space inside the leaf and ambient air surrounding the leaf and (2) the exchange velocity (m s^{-1}) relating the deposition or emission flux to the concentration gradient.[24,25] Deposition occurs if the OVOC mixing ratio

Received: November 12, 2023
Revised: January 19, 2024
Accepted: January 26, 2024
Published: March 18, 2024

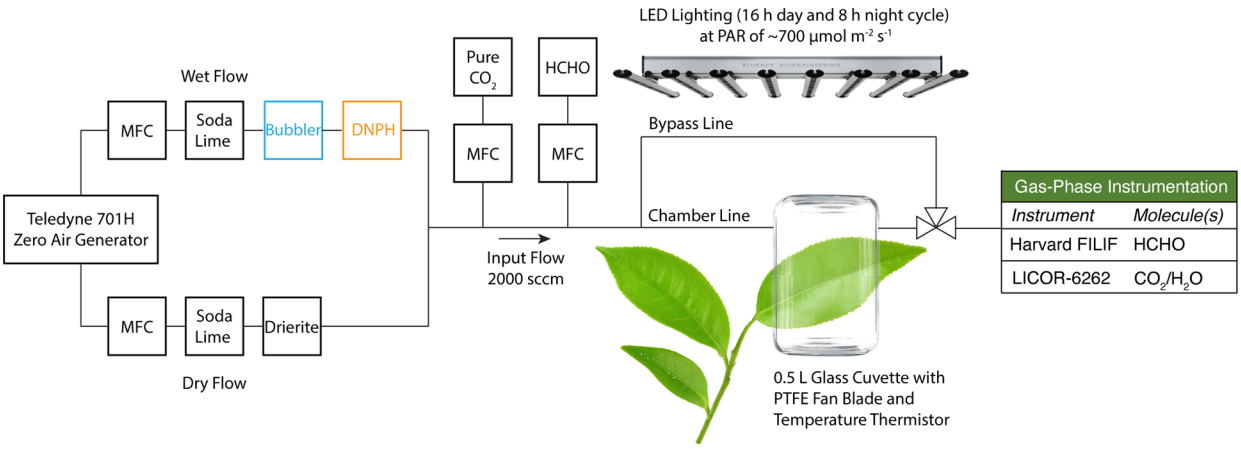

Figure 1. Schematic of the custom-built leaf cuvette system used for HCHO bidirectional exchange experiments.

outside the leaf is greater than inside the leaf; whereas, emission occurs in the converse case. The mixing ratio at which there is zero net OVOC flux to or from the leaf is defined as the compensation point (CP). Other OVOCs that exhibit bidirectional exchange include ethanol, acetaldehyde, acetic acid, and formic acid.[2]

While the existence of a HCHO CP is well-established, there exists considerable uncertainty as to how much the exchange of HCHO with foliage contributes to the HCHO flux to or from the biosphere.[26−28] For example, DiGangi et al. observed mixing ratios ranging from ∼1 to 2.5 ppbv HCHO in a Ponderosa Pine forest canopy. They additionally identified a missing positive HCHO flux from a Ponderosa Pine forest and postulated that this could be attributable in part to direct emissions of HCHO from the pine trees.[26] Over cropland, Kaiser et al. measured mixing ratios of ∼2−4 ppbv HCHO at low altitude (i.e., <100 m). They also hypothesized a direct biogenic emission source of HCHO as a missing source of HCHO in their simulations.[27] Uncertainties in HCHO exchange with foliage are due in part to limitations from previous studies trying to characterize the HCHO CP and its exchange velocity using (1) field studies[17−22] with limited statistics or variable environmental conditions (e.g., leaf temperature, light, relative humidity, etc.) or (2) laboratory studies[23] using high mixing ratios of HCHO (>10 ppbv HCHO) not generally observed in rural forests. For example, the HCHO CP for the genus *Quercus* has a reported range between 1 and 20 ppbv, spanning an order of magnitude.[18,23] As such, controlled studies are necessary to quantify HCHO exchange with foliage across a range of environmental conditions.

In this work, leaf-level studies on deciduous northern red oak (*Quercus rubra*) and evergreen Leyland cypress (*Cupressus* × *leylandii*) saplings are performed under a controlled laboratory environment. Using ambient mixing ratios of HCHO (i.e., 0−6 ppbv) and a statistically robust sampling of leaves from both species, the magnitude of the HCHO CP and its exchange velocity are constrained across a range of temperatures and relative humidities (RHs). The observed range of water stomatal conductances further allows for an evaluation of which dry deposition resistor framework parameters are best suited for HCHO.[6,29] Finally, the atmospheric implications of these findings are discussed.

2. MATERIALS AND METHODS

2.1. Tree Type and Care. Northern red oaks (*Q. rubra*; Cold Stream Farms; 1−2-year-old saplings) were chosen as the deciduous tree for this study due to their prominence across the entire eastern U.S. and Canada (Figure S1).[30] *Q. rubra* saplings were received as bare root and subsequently potted in PVC tubes containing Fafard 3B soil mix. Additionally, Leyland cypress trees (*C.* × *leylandii*; Home Depot; 1−3-year-old saplings) were chosen as the evergreen species because they were easy to procure during the winter and their leaves fit well in the experimental setup. *C.* × *leylandii* saplings were received and experimented on as is. Trees were maintained in the Harvard Organismic and Evolutionary Biology (OEB) Greenhouse and brought into the laboratory for at least 2 weeks to acclimate. Once in the laboratory, the saplings were given 500 mL of tap water ∼2 times a week when the soil dried (determined by using an XLUX Soil Moisture Meter). Saplings were fertilized with water-soluble Miracle-Gro fertilizer monthly.

2.2. Dynamic Leaf Cuvette System. Figure 1 shows a schematic of the custom-built, dynamic (i.e., continuous air flow) leaf cuvette system used to study HCHO bidirectional exchange in the laboratory. The centerpiece of the system is a cuvette assembly based on the design of Harley et al. and Nagalingam et al.[31,32] In short, a 0.5 L cuvette (Allen Scientific Glass) composed of two separable halves was fabricated from borosilicate glass to eliminate the need for any plastics that may emit HCHO or other VOCs. In the lower half of the cuvette, a cut groove provides space for an O-ring that is coated in Fluoropel to minimize VOC outgassing. The O-ring creates an airtight seal and provides a soft cushion for the leaf when the two halves of the cuvette are clamped together. To ensure turbulent mixing and minimize aerodynamic resistance,[33] a fan fabricated from PTFE foam is located at the base of the cuvette.

The glass cuvette sits flush on an aluminum plate lying above two Peltier thermoelectric coolers (Custom Thermoelectric; 12711-5P31-15CQ; RTV Moisture Sealed) mounted on a bonded-fin heat sink with thermal epoxy. A thermistor (Oven Industries; TR67) was placed inside the cuvette alongside the leaf to monitor and allow the associated PID temperature controller to maintain the temperature to within ±0.2 °C of a desired set point. The entire assembly was mounted on top of a tripod that makes the cuvette assembly portable and ensures that its weight is not placed on a leaf or plant.

https://doi.org/10.1021/acsearthspacechem.3c00325
ACS Earth Space Chem. 2024, 8, 723−733

PFA tubing connects the inlet and outlet of the glass cuvette to the rest of the setup and is used everywhere in the setup given that PFA does not outgas HCHO. An automated valve system also allows for connected instrumentation to sample from either the chamber (i.e., cuvette) or the bypass line at any given time. Above the cuvette, specialized LED lighting (Fluence Bioengineering; SPYDRx PLUS) simulates the visible wavelengths of the solar spectrum, and a timer automatically controls the lighting cycle (16 h day and 8 h night). Daytime experiments are performed at a photosynthetic photon flux density (PPFD) of ∼700 μmol m^{-2} s^{-1}.

A continuous source of zero air is provided to the cuvette assembly via a zero-air generator (ZAG; Teledyne 701H), but it produces several tens of parts per million of CO_2 from conversion of VOCs inside its catalytic converter. To address this, in-line soda lime columns are used to remove the excess and variable CO_2 levels in both the dry and wet airstreams. Since H_2O is produced as CO_2 reacts with the soda lime, a desiccant column (Drierite) is placed in the dry airstream to provide greater control over humidity levels inside the cuvette. The wet airstream contains a custom-made bubbler with glass frits, followed by a DNPH cartridge to remove trace amounts of HCHO from the humidified air. Average CO_2 mixing ratios between 400 and 430 ppmv are held steady through the introduction of a small flow (<5 sccm) of pure CO_2 (Airgas). Measurements by a LICOR-6262 in absolute mode (calibrated weekly) indicate stable CO_2 measurements to within ±1 ppmv and H_2O measurements to within ±0.1 ppthv. These small changes in CO_2 and H_2O are negligible compared to actual changes in leaf physiology as recorded from H_2O emission and CO_2 uptake fluxes.

2.3. HCHO Cuvette Characterization. Measurements of HCHO in this study are performed using the Harvard FIber Laser-Induced Fluorescence (FILIF) instrument (calibrated monthly).[26,34−36] Briefly, FILIF detects HCHO by exciting gas-phase HCHO with a narrow-bandwidth UV fiber laser at 353 nm, and a photomultiplier tube (PMT) covered by a long-pass filter measures the resulting fluorescence at wavelengths greater than 370 nm. The difference in power-normalized photon counts between the online and offline HCHO spectral features is proportional to the HCHO mixing ratio in the gas sample. The measurement of HCHO by laser-induced fluorescence has no known interference from other molecular species and is not impacted by changes in humidity.

HCHO is introduced to the cuvette system from a 5 ppmv HCHO gas cylinder (Airgas) and diluted down to ambient mixing ratios between 0 and 6 ppbv HCHO with the humidified airstream from the ZAG.[26,37] Mixing ratios in the setup are generally stable to within ±10−30 pptv of HCHO. Additionally, results from several blank experiments show that an empty glass cuvette is not a significant source or sink of HCHO in the setup. Figure S2 indicates that the chamber and bypass HCHO mixing ratios are within ±1% of each other with a small offset of around 30 or 40 pptv of HCHO (with lights both on and off). These differences are negligible compared to when a leaf is exposed to HCHO and indicate a negligible amount of HCHO wall loss in the glass cuvette. Moreover, the results provide confidence that the overflows used during experiments did not allow HCHO-laden room air to enter the cuvette assembly.

2.4. Protocol and Types of Experiments. For any given experiment, the leaf was allowed to acclimate within the cuvette overnight to avoid potential interferences from mechanical leaf stress.[38] The leaf was exposed to 15 different HCHO mixing ratios for 15 min each (12 and 3 min of chamber and bypass sampling, respectively) to ensure that HCHO in the cuvette reached steady-state. To prevent hysteresis, mixing ratios of HCHO were randomized such that the leaf was exposed to varying levels of high or low HCHO throughout the experiment as opposed to monotonically increasing or decreasing the levels of HCHO. CO_2 and H_2O differences were measured by the LICOR-6262 every three HCHO steps (4 min each for chamber and bypass sampling) to quantify how much the H_2O emission or CO_2 uptake fluxes were changing over time. Changes in H_2O stomatal conductance over the total length of an experiment (∼4 h) were within 20%. The 0.5 L leaf cuvette and 2000 sccm total airflow (measured using a Model 4140 F flowmeter; TSI Incorporated) yielded a residence time of 15 s within the cuvette. This was sufficient for Harvard FILIF and LICOR-6262 to resolve a signal between the chamber and bypass lines.

Table 1 shows a synopsis of the different types of experiments performed with additional details from individual leaves included in Tables S1 and S2. To summarize, experiments were conducted under the following conditions: (i) standard base case 30 °C, 40% RH, and a PPFD of ∼ 700 μmol m^{-2} s^{-1} for (a) oak and (b) cypress trees, (ii) lights off experiments at 30 °C and 40% RH for (a) oak and (b) cypress trees, (iii) 22 °C for oak trees, (iv) 35 °C for oak trees, and (v) 30 °C and 70% RH for oak trees. Experiment types (i) and (ii) were designed to test the influence of tree species and stomatal opening on HCHO CP and exchange, while experiment types (iii)−(iv) and (v) tested the impact of temperature and humidity on HCHO CP and exchange, respectively. In total, 53 experiments measuring the HCHO exchange between oak and cypress leaves were performed.

Table 1. Summary of HCHO Compensation Point and Exchange Velocity Experiments with Oak and Cypress Trees

ID	tree type	temperature (°C)	RH[a] (%)	lights	number of experiments
ia	oak	30	40	on	10
ib	cypress	30	40	on	7
iia	oak	30	40	off	6
iib	cypress	30	40	off	6
iii	oak	22	60	on	9
iv	oak	35	30	on	8
v	oak	30	70	on	7

[a]All experiments had H_2O volume mixing ratios at 16.5 ppthv except (v) at 30.0 ppthv H_2O.

2.5. Calculations and Statistics. *2.5.1. Calculation of HCHO Compensation Point.* Exposing a given oak or cypress leaf to varying mixing ratios of HCHO allowed calculation of the CP by plotting the measured HCHO mixing ratio from the bypass line against the HCHO mixing ratio measured from the chamber (i.e., the cuvette) for each step.[39] An illustrative example of a red oak leaf is shown in Figure 2a, where the error bars on each point represent the standard error of the mean for any given HCHO step (after outlier removal has taken place).

The experimental data for a given leaf are fit using a bivariate linear regression (York fit) that takes into account errors in the independent and dependent variables.[40] The linearity of the fit is justified by checking for the normality of the residuals (using

https://doi.org/10.1021/acsearthspacechem.3c00325
ACS Earth Space Chem. 2024, 8, 723−733

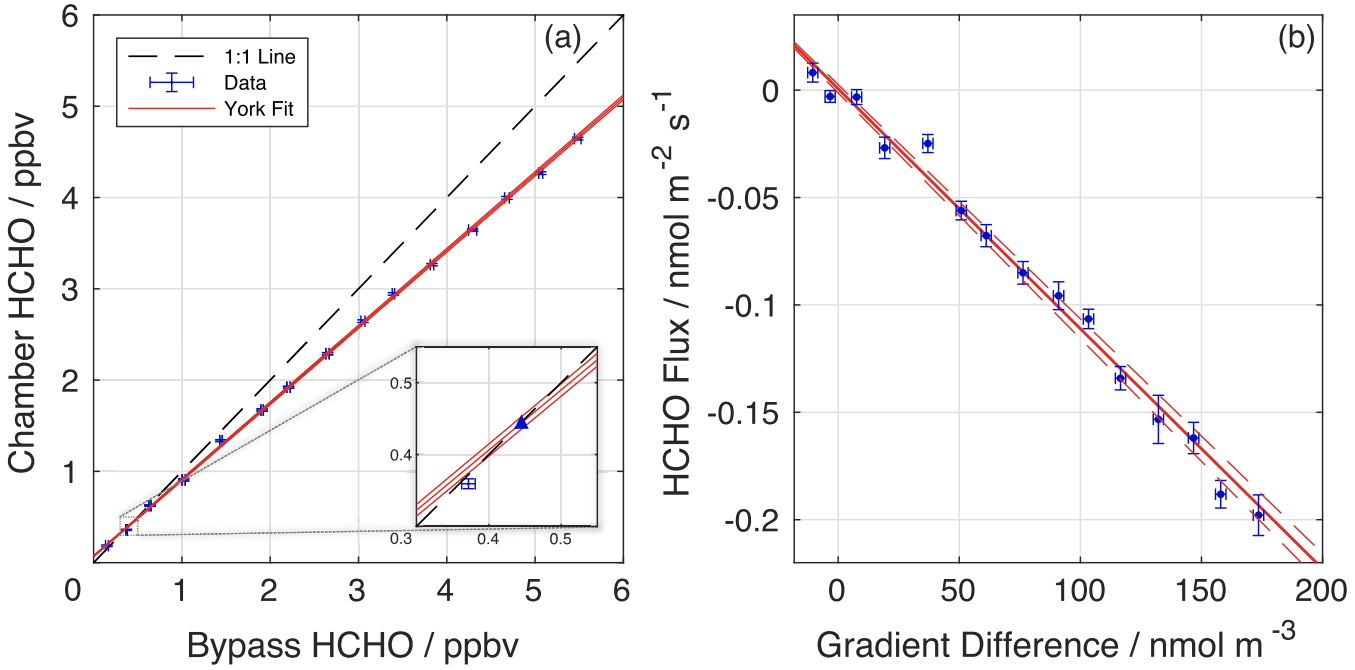

Figure 2. Example plots for determining the (a) HCHO CP and (b) $v_{ex,HCHO}$ for a given leaf. (a) HCHO CP was determined by finding the intercept of the bivariate linear regression (York fit) of the bypass versus chamber HCHO mixing ratios with the 1:1 line. The inset is a zoomed in view of where the fit intercepts the 1:1 line (indicated by the triangle at 0.44 ± 0.05 ppbv HCHO). (b) $v_{ex,HCHO}$ (0.1117 ± 0.0026 cm s^{-1}) was calculated as the slope of the York fit between the HCHO flux and the gradient difference between the ambient HCHO mixing ratio in the cuvette and the HCHO CP.

the Shapiro-Wilk normality test in R) and uniform variance and homoscedasticity (using ncvTest in R). If the fit fails one of these statistical tests (i.e., the p value was <0.05), then the residuals are visualized to assess their uniform variance or normality (the latter via a Q−Q plot using a normal distribution for comparison). Visualizing the residuals shows which point(s) cause the fit to fail the statistical tests and provides statistical justification for their removal. No more than 2 points out of 15 were removed from each individual leaf experiment.

With a statistically justified linear fit, the CP corresponds to the mixing ratio where the York fit crosses the 1:1 line. The calculated standard errors for the values of the York fit slope and intercept are used to calculate the error in the CP.

2.5.2. Calculation of Total HCHO Exchange Velocity. For each mixing ratio step within an experimental run, the exchange flux of HCHO, $F_{ex,HCHO}$, for a leaf inside the cuvette was calculated using the following equation:

$$F_{ex,HCHO} = \frac{Q_{molar}}{A} \cdot ([HCHO]_{chamber} - [HCHO]_{bypass}) \quad (1)$$

where Q_{molar} is the molar flow rate (mol s^{-1}), A is the one-sided leaf area (m^2), and $[HCHO]_{chamber}$ and $[HCHO]_{bypass}$ are unitless mole fractions of the HCHO mixing ratio leaving the chamber and bypass lines, respectively. The areas for all leaves were calculated nondestructively by importing a high-resolution photo of flat leaves into an open-source Python script (Easy Leaf Area).[41]

For a compound such as HCHO exhibiting bidirectional exchange, the exchange flux is dependent on the HCHO concentration gradient between the ambient air and the intercellular air space within the leaf as shown in the following equation:

$$F_{ex,HCHO} = -v_{ex,HCHO}[C_a - C_i] \quad (2)$$

where C_a and C_i are the concentrations of HCHO in the air outside and inside of the leaf, respectively, and $v_{ex,HCHO}$ is the total HCHO exchange velocity (m s^{-1}). The concentration of HCHO in the intercellular air space cannot be measured directly with the cuvette setup, but the HCHO CP for a given leaf can be used as the proxy for the internal concentration of HCHO and is assumed to be constant throughout the experiment (i.e., not affected by the mixing ratio of HCHO being exposed to the leaf). This assumption is likely justified, given that the leaf is exposed to HCHO mixing ratios that are no different than what the leaf regularly would encounter outside. Thus, excess levels of HCHO above the CP should be readily metabolized by the leaf. Given this assumption, eq 2 can be rewritten as

$$F_{ex,HCHO} = -v_{ex,HCHO}[C_a - C_{CP}] \quad (3)$$

where C_{CP} is the value of the HCHO CP for a given leaf in units of molar concentration (mol m^{-3}). Using eq 3, the slope of the line between $F_{ex,HCHO}$ and $[C_a - C_{CP}]$ can be used to experimentally determine $v_{ex,HCHO}$ for each leaf (example shown in Figure 2b). Accordingly, all $v_{ex,HCHO}$ values were determined using the slope magnitude and its standard error from a York fit, whose linearity was justified using the same statistical methodology as for the HCHO CP calculation.

2.5.3. Calculation of HCHO Total Foliar Surface Resistances. The same resistor framework for dry depositing gas-phase species can be applied to compounds that exhibit bidirectional exchange. In brief, transport of gases depositing to a surface can be simplified into three layers to simplify the underlying microphysics. First, there is transport of the gas through the aerodynamic surface layer, which is governed by turbulent diffusion. The second step is transport through the

https://doi.org/10.1021/acsearthspacechem.3c00325
ACS Earth Space Chem. 2024, 8, 723−733

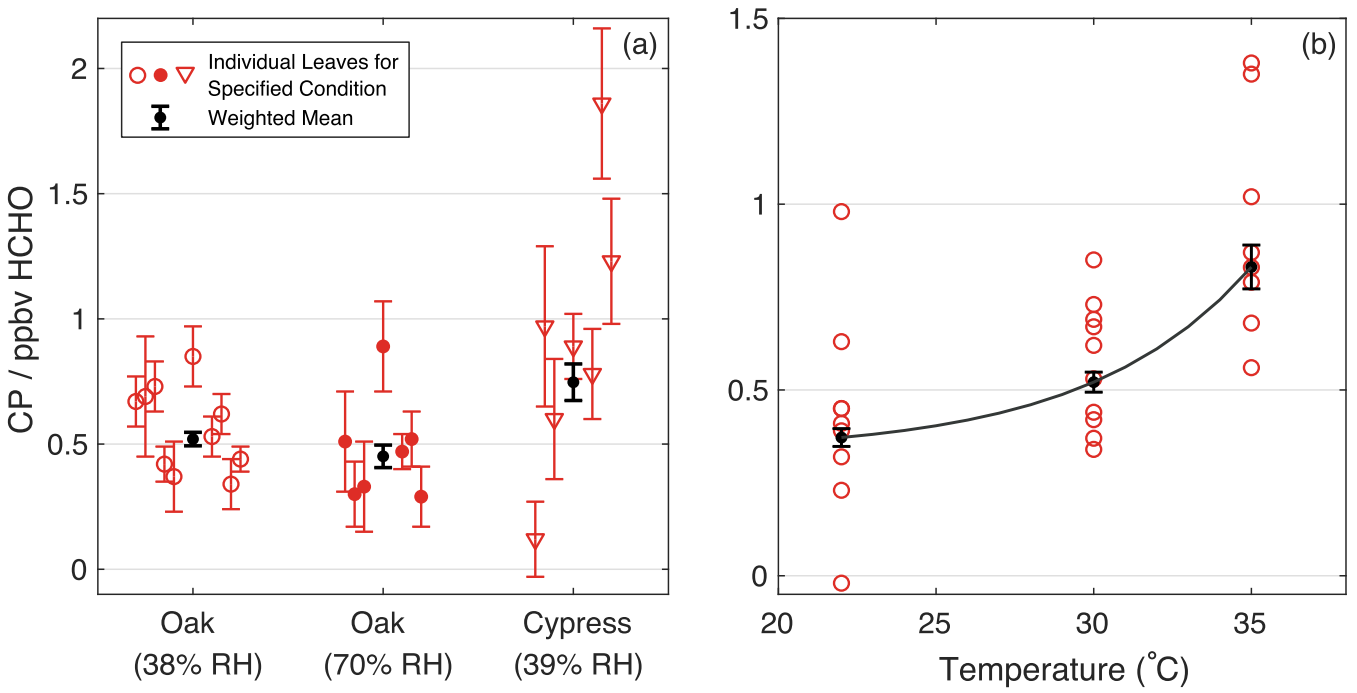

Figure 3. Comparison of oak and cypress HCHO CPs under different experimental conditions: (a) relative humidity and tree species and (b) temperature. While not shown graphically in (b), the error bars for each individual leaf CP (red) are derived from the uncertainty in their corresponding York fit and are explicitly used in the calculation of the weighted mean CP for each experimental condition (black). The parametrization in eq 8 describes the solid black line through the weighted means at each temperature in (b).

boundary layer, which is a layer that is a few millimeters thick above the surface, where the air is mostly stationary. Transport through this layer occurs via molecular diffusion. The final layer is the surface itself, and deposition of a trace gas to the surface is controlled by factors such water solubility, volatility, diffusivity, and reactivity of the trace gas in addition to the composition of the leaf surface.[42,43] It is useful to conceptualize these three layers as electrical resistors in series with one another such that their sum (R_{total}) governs the speed of exchange as shown in the following equation:

$$R_{total} = R_a + R_b + R_c = \frac{1}{v_{ex}} \quad (4)$$

where R_a is the aerodynamic surface layer resistance, R_b is the boundary layer resistance, and R_c is the surface resistance. By definition, the inverse of the R_{total} is the total exchange velocity.

The HCHO total foliar surface resistance ($R_{c,HCHO}$) can be derived from the experimentally determined $v_{ex,HCHO}$ if R_a and $R_{b,HCHO}$ are known. $R_{b,HCHO}$ was experimentally determined by suspending activated charcoal (ErtelAlsop) that was cut in the shape of an oak leaf inside the cuvette. Since the surface resistance of the activated charcoal is assumed to be zero ($R_{c,HCHO}$ = 0 s m^{-1}), the boundary layer is the only limiting resistance that determines the deposition of HCHO in this case.[44] The same protocol and statistics for obtaining the total HCHO exchange velocity with actual leaves were followed for the activated charcoal at 25, 30, and 35 °C, and the results are shown in Table S3. Since the cuvette system is well-mixed and turbulent, R_a is assumed to equal zero. Even if R_a was not zero, there would be no impact on the derivation of $R_{c,HCHO}$ since the charcoal leaf experiments would simply have combined contributions of R_a and $R_{b,HCHO}$.

After taking the inverse of the total HCHO exchange velocity ($v_{ex,HCHO}$) to calculate $R_{total,HCHO}$, the appropriate $R_{b,HCHO}$ is subtracted from $R_{total,HCHO}$ for a given leaf to obtain $R_{c,HCHO}$. While errors for $v_{ex,HCHO}$ are Gaussian, the assumptions of Gaussian error propagation are no longer met when taking the inverse of $v_{ex,HCHO}$ if the error ($\delta v_{ex,HCHO}$) is close in magnitude to the value of $v_{ex,HCHO}$. As a result, a Monte Carlo approach was used to propagate error on $R_{total,HCHO}$ and, subsequently, $R_{c,HCHO}$.[45] While Gaussian-like behavior was still obtained for low resistances of HCHO, non-Gaussian behavior was observed as the resistances increased in magnitude.

2.5.4. Calculation of H_2O Stomatal Resistances. H_2O emission fluxes during an experimental run were calculated according to eq B5 from von Caemmerer and Farquhar,[46] which takes into account that the emission of water vapor, E_{H_2O} (mol m^{-2} s^{-1}), from the leaf increases the flow out of the cuvette by a slight amount as shown by

$$E_{H_2O} = \frac{Q_{molar}}{A} \cdot \left(\frac{[H_2O]_{chamber} - [H_2O]_{bypass}}{1 - [H_2O]_{chamber}} \right) \quad (5)$$

Having obtained the H_2O emission flux from the leaf, the total conductance of H_2O, g_{total,H_2O}, is then calculated using eq B14 from von Caemmerer and Farquhar as shown by

$$g_{total,H_2O} = \frac{E_{H_2O} \cdot (1 - \overline{w})}{(w_i - w_a)} \quad (6)$$

where w_i and w_a are the mole fractions of water vapor inside the leaf and in the air surrounding the leaf, respectively, and $\overline{w} = (w_i + w_a)/2$. While the mole fraction of water vapor surrounding the leaf is measured experimentally by the LICOR, the mole fraction of water vapor inside the leaf is the saturation water vapor pressure (calculated using the Goff-Gratch equation) divided by the total chamber pressure

https://doi.org/10.1021/acsearthspacechem.3c00325
ACS Earth Space Chem. 2024, 8, 723−733

(101.325 kPa) since the RH inside the leaf is assumed to be 100%. Conversion of g_{total,H_2O} from units of mol m^{-2} s^{-1} to m s^{-1} can be accomplished by multiplying by RT/P where R is the gas constant, T is the temperature, and P is the pressure. Taking the inverse of gives the total H_2O resistance (R_{total,H_2O}). A Monte Carlo approach was utilized to propagate the error on R_{total,H_2O} and subsequent calculated quantities as was done similarly for the error on $R_{total,HCHO}$ and $R_{c,HCHO}$ in Section 2.5.3.

While each experimental run allowed for the total H_2O conductance (or resistance) to be obtained, many models tend to calculate the H_2O stomatal conductance (or resistance) for use in dry deposition parametrizations. As shown in eq 7, the H_2O stomatal resistance (R_{s,H_2O}) is related to R_{total,H_2O} by

$$R_{total,H_2O} = R_{b,H_2O} + R_{s,H_2O} \quad (7)$$

where R_{b,H_2O} is the boundary layer resistance to water vapor. This was experimentally determined for the leaf cuvette setup by wetting several pieces of Whatman filter paper (cut out in the shape of an oak and cypress leaf) with DI water and suspending the saturated filter paper cutouts in the leaf cuvette.[47] R_{b,H_2O} could then be calculated using eqs 5 and 6. This experiment was performed multiple times for each of the temperatures probed during the study (22, 30, and 35 °C), with results shown in Table S4. The determination of R_{b,H_2O} and its subsequent subtraction from R_{total,H_2O} allowed for the value of R_{s,H_2O} to be calculated for all oak and cypress leaves in this study.

3. RESULTS AND DISCUSSION

3.1. Effects of Humidity, Tree Species, and Temperature on HCHO Compensation Point. Individual HCHO CPs were grouped together based on humidity, tree species, and temperature to assess whether these environmental conditions had any statistically significant impact on the magnitude of the HCHO CP. Figure 3a shows the HCHO CPs measured for oak at 40 and 70% RH and cypress at 40% RH in addition to their weighted means. To test whether the HCHO CPs were statistically different, one-way analysis of variance (ANOVA) tests were performed (described in the Supporting Information). Based on the ANOVA results in Table S5, the 40 and 70% RH CPs and the oak and cypress CPs are not statistically different from each other, suggesting that the HCHO CP is independent of these RHs and tree species.

Figure 3b shows individual oak HCHO CPs (and the corresponding weighted means) at different temperatures but all at the same RH (40%) and PPFD (~700 μmol m^{-2} s^{-1}). ANOVA testing indicates that one of the temperature groupings is statistically different from the others (p value < 0.05). Further analysis with the TukeyHSD test indicates that the HCHO CPs at 35 °C were statistically different from those at 22 and 30 °C. Additionally, there is an observed exponential rise in the HCHO CP as the temperature increases, which is similar to what was previously reported for acetaldehyde.[48] A temperature parametrization valid between 22 and 35 °C and suitable for models was derived for the HCHO CP as shown in the following equation:

$$CP_{HCHO}(T) = (0.332 \pm 0.051) + (0.189 \pm 0.068) \cdot e^{(0.194 \pm 0.062)(T-30)} \quad (8)$$

The resulting HCHO CPs between 22 and 35 °C range from 0.3 to 0.9 ppbv, accounting for the 95% confidence intervals. The HCHO CP in this study is lower than HCHO mixing ratios observed in Eastern U.S. forests (1.5−6 ppbv),[49,50] which suggests that foliage would act as a net sink of HCHO rather than as an emission source.

Past determinations of a HCHO CP have been reported over a large range. Rottenberger et al. reported a HCHO CP of 0.49 and 0.21 ppbv for *Hymenaea courbaril* and *Apeiba tibourbou*, respectively, in the field.[21] Kesselmeier et al. reported a CP of 1 ppbv HCHO for *Quercus pubescens* at a field site near Montpellier, France.[18] Interestingly, Seco et al. reported a HCHO CP around 20 ppbv for both *Pinus halepensis* and *Quercus ilex* in the laboratory.[23] Thus, for the same genus, *Quercus*, the HCHO CP ranged from a possible 1 to 20 ppbv. Our experimental HCHO CP results agree in magnitude with Rottenberger and Kesselmeier even though these studies were performed in the field with mature trees (i.e., not saplings). While leaf age has been shown to impact methanol emissions,[51] there does not appear to be conclusive evidence that this is the case for the HCHO CP. As such, more studies should investigate the potential impact of leaf and tree age on the HCHO CP. The disagreement with Seco et al. is likely due to a range of factors. First, the trees in their study were exposed to high "urban" levels of HCHO ranging from 4 to 68 ppbv, which could potentially increase the internal HCHO concentration in the trees after deposition and bias the CP high. Second, the Seco study used PTR-MS to measure HCHO, which is subject to humidity corrections.[52−54] Third, the Seco study used different tree species than the current work, which can lead to differences in HCHO CP based on the complexity and uncertainty involved in leaf C1 biochemical mechanisms.[55] While this work shows that *Q. rubra* and *C.* × *leylandii* have similar HCHO CP, future work should investigate several different tree species to further constrain the impact that tree species have on the HCHO CP. Lastly, the Seco study (ref 23) may have had ambient "urban" levels of O_3 in their setup, which can bias the HCHO CP high since O_3 can (1) react with other VOCs in the cuvette depending on the residence time of air, (2) react heterogeneously on the leaf, and (3) produce a positive bias in the PTR-MS.[56]

3.2. Comparison of Experimentally Derived $R_{c,HCHO}$ to Other Deposition Schemes. Having calculated R_{s,H_2O} and $R_{c,HCHO}$ for each of the leaves experimented on in this study (see Table 1 for experimental conditions), their corresponding probability distributions (representing their error from using a Monte Carlo error propagation approach) were fit using an Epanechnikov kernel distribution. This allowed for a parametrization of R_{s,H_2O} versus $R_{c,HCHO}$ to be derived from the experimental data using a bivariate linear regression (York fit) with corresponding Monte Carlo approach (N = 5000 runs).[45,57−59] Figure 4 shows the experimental data used with the corresponding parametrization shown in the following equation:

$$R_{c,HCHO}(R_{s,H_2O}) = (1.62 \pm 0.06) \cdot R_{s,H_2O} + (-223 \pm 48) \quad (9)$$

Only data points with an R_{s,H_2O} smaller than 3000 s m^{-1} were used to ensure normality since data points which had R_{s,H_2O} of 3000 s m^{-1} or greater (and therefore not used in the parametrization) had low signal (Figure S3). Given the range of R_{s,H_2O} used to generate this parametrization (i.e., 500−3000

https://doi.org/10.1021/acsearthspacechem.3c00325
ACS Earth Space Chem. 2024, 8, 723−733

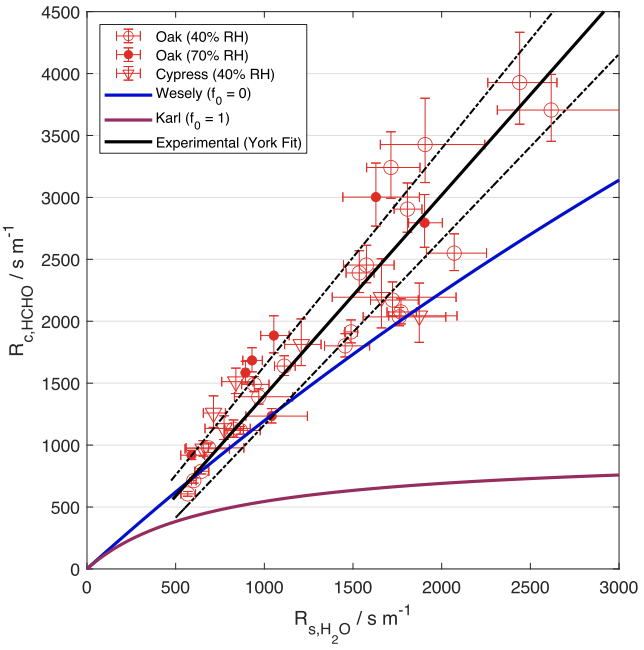

Figure 4. Bivariate linear regression (York fit) of experimentally obtained $R_{c,HCHO}$ versus their corresponding R_{s,H_2O}. Error bars on the fit denote the 95% confidence interval. Only data with a H_2O stomatal resistance of 3000 s m^{-1} or smaller (conversely a H_2O stomatal conductance of 15 mmol m^{-2} s^{-1} or greater) are shown and used for determining experimental fit. Comparisons to Wesely (1989) and Karl (2010) HCHO dry deposition parametrizations are also shown for comparison.

s m^{-1}), extrapolating above or below this range to obtain $R_{c,HCHO}$ with eq 9 is not advised.

The experimentally measured $R_{c,HCHO}$ can also be used to assess estimates of $R_{c,HCHO}$ from other dry deposition schemes as a function of R_{s,H_2O}. For foliage, exchange can happen either via the cuticle or through the stomata. While uptake via the cuticle can be described by a single resistor (R_{cut}), exchange via the stomata is composed of two resistors in series: R_{stom} (representing resistance to diffusion through the stomatal pore itself) and R_{meso} (representing resistance to dissolution in the moist tissues of the mesophyll). As a result, $R_{c,HCHO}$ is comprised of the cuticular ($R_{cut,HCHO}$) as well as the stomatal and mesophyllic ($R_{stom,HCHO} + R_{meso,HCHO}$) pathways acting as parallel resistors:

$$R_{c,HCHO} = \left(\frac{1}{R_{cut,HCHO}} + \frac{1}{R_{stom,HCHO} + R_{meso,HCHO}} \right)^{-1} \quad (10)$$

Specific parametrizations of R_{cut}, R_{stom}, and R_{meso} for OVOCs were developed by Wesely (1989) with updates by Karl et al. and Nguyen et al.[3,6,29] For HCHO, the Wesely parametrizations for $R_{cut,HCHO}$, $R_{stom,HCHO}$, and $R_{meso,HCHO}$ are

$$R_{stom,HCHO} = \left(\frac{D_{H_2O}}{D_{HCHO}} \right) \cdot R_{s,H_2O} \quad (11)$$

$$R_{meso,HCHO} = \left(\frac{H^*}{3000} + 100 \cdot f_0 \right)^{-1} \quad (12)$$

$$R_{cut,HCHO} = r_{lu} \cdot \left(\frac{1}{10^{-S} \cdot H^* + f_0} \right) \quad (13)$$

where $D_{H_2O}/D_{HCHO} = 1.29$ is a ratio of the molecular diffusivity of water to HCHO, R_{s,H_2O} is the stomatal resistance of H_2O in units of s m^{-1}, H^* is the effective Henry's law constant for HCHO (3400 ± 200 M atm^{-1}),[60] and f_0 is the reactivity factor (between 0 and 1). In the original Wesely scheme, $f_0 = 0$ for HCHO, though the update by Karl et al. suggested $f_0 = 1$ was more appropriate for HCHO and several other OVOCs. Finally, r_{lu} is an empirical factor that considers seasonality as well as land use type. For vegetation in the summer, r_{lu} = 2000 s m^{-1} is an appropriate value.

While $R_{stom,HCHO}$ is the same in both the Wesely and Karl parametrizations, the two parametrizations differ in $R_{meso,HCHO}$ and $R_{cut,HCHO}$ given the different assumptions for the value of f_0. In the Wesely scheme, $R_{cut,HCHO}$ = ~60 000 s m^{-1} as opposed to ~1900 s m^{-1} for the Karl scheme. Moreover, Wesely predicts an $R_{meso,HCHO}$ of ~1 s m^{-1}; whereas, Karl predicts over an order of magnitude smaller resistance of 0.01 s m^{-1}.

Using eq 10, the Wesely and Karl parametrizations for $R_{c,HCHO}$ were calculated as a function of R_{s,H_2O} and overlaid on Figure 4 to compare with the experimentally observed $R_{c,HCHO}$. While exact agreement with a parametrization is not expected for a single leaf due to natural variability, it is notable that the experimentally observed $R_{c,HCHO}$ are in closer agreement with the Wesely parametrization compared to the more recently updated Karl parametrization over the range of R_{s,H_2O} obtained experimentally. The experimental data are unable to distinguish between the Wesely and Karl parametrizations for R_{s,H_2O} < 500 s m^{-1} since that would require extrapolation from the experimental data set.

While the stomatal conductance of H_2O (g_{s,H_2O}) never reached zero during any of the dark experiments, an experimental $R_{cut,HCHO}$ can be approximated when the leaf stomata were relatively shut. For R_{s,H_2O} > 10000 s m^{-1} as shown in Figure S3, experimentally obtained $R_{c,HCHO}$ ranged from ~8000 to 52 000 s m^{-1} with a median value of ~30 000 s m^{-1}. Given that $R_{c,HCHO} \approx R_{cut,HCHO}$ for large R_{s,H_2O}, a possible median lower bound for the magnitude of $R_{cut,HCHO}$ is 30 000 s m^{-1}, which is similar in magnitude to the Wesely estimate of $R_{cut,HCHO}$ of ~60 000 s m^{-1}. Additionally, assuming an $R_{cut,HCHO}$ of 30 000 s m^{-1} and evaluating eq 9 at R_{s,H_2O} of 500 and 3000 s m^{-1}, the cuticular pathway contributes 2 and 15%, respectively, to $R_{c,HCHO}$. This indicates that the cuticle plays a negligible to a limited role in HCHO exchange and that HCHO emission and uptake are controlled by the stomata. Branch enclosure measurements of trees in a tropical forest corroborate our result that HCHO uptake is stomatally controlled.[21] However, this study is the first to parametrize the HCHO total foliar surface resistance as a function of H_2O stomatal resistance for incorporation into models.

With an experimentally obtained median estimate for the value of $R_{cut,HCHO}$ and using eq 11 for $R_{stom,HCHO}$, experimental values for $R_{meso,HCHO}$ can also be calculated for each leaf. Figure S4 shows the corresponding $R_{meso,HCHO}$ and $R_{stom,HCHO}$ for all experiments with a H_2O stomatal resistance less than 3000 s m^{-1}. While error bars representing the 95% confidence interval overlap with $R_{meso,HCHO}$ predicted by both Wesely (~1 s m^{-1})

https://doi.org/10.1021/acsearthspacechem.3c00325
ACS Earth Space Chem. 2024, 8, 723−733

and Karl (0.01 s m^{-1}) for a majority of the experiments, there were a non-negligible number of leaves (N = 15 out of 36) where even the confidence interval bounds on $R_{meso,HCHO}$ are substantially higher than the $R_{meso,HCHO}$ predicted by either model framework for dry deposition. The effective Henry's Law constant for HCHO (3400 ± 200 M atm^{-1}) would have to be lower by nearly 2 orders of magnitude before the Wesely dry deposition parametrization would become comparable in magnitude to many of our observed high $R_{meso,HCHO}$. This suggests a dependence of $R_{meso,HCHO}$ on other factors (perhaps biological) that are currently unaccounted for in dry deposition frameworks to explain some of the observed higher $R_{meso,HCHO}$ values.[7] Nevertheless, the experimental data points support choosing f_0 = 0 as in the Wesely scheme for HCHO as opposed to f_0 = 1 as recommended by Karl et al.

3.3. Atmospheric Implications. The laboratory HCHO CP and leaf resistance results have a direct impact on the magnitude of the deposition flux (eq 2) as a sink of HCHO. Experimental results show a nonzero HCHO CP (i.e., $C_i \neq 0$) and support the use of f_0 = 0 for calculating mesophyllic and cuticular resistances. As such, HCHO deposition fluxes calculated using these laboratory recommendations would be smaller than fluxes calculated by models that use f_0 = 1 and C_i = 0. Figure 5 shows the percent difference in the HCHO deposition flux when using an f_0 = 0 and C_i = 0.52 ppbv (HCHO CP at 30 °C) relative to f_0 = 1 and C_i = 0 ppbv over a range of ambient HCHO mixing ratios and R_{s,H_2O} commonly encountered in a pristine forest. Only ambient mixing ratios in which both scenarios predict deposition are compared. During the day when R_{s,H_2O} is lower and ambient HCHO is higher, calculated HCHO deposition fluxes using an f_0 = 0 and a C_i = 0.52 ppbv are generally 20−50% lower than fluxes calculated using f_0 = 1 and a C_i = 0 ppbv. However, fluxes can be 80−90% lower at nighttime when R_{s,H_2O} is high and ambient HCHO is low, although the absolute magnitude of the deposition flux would be lower at night than during the day.

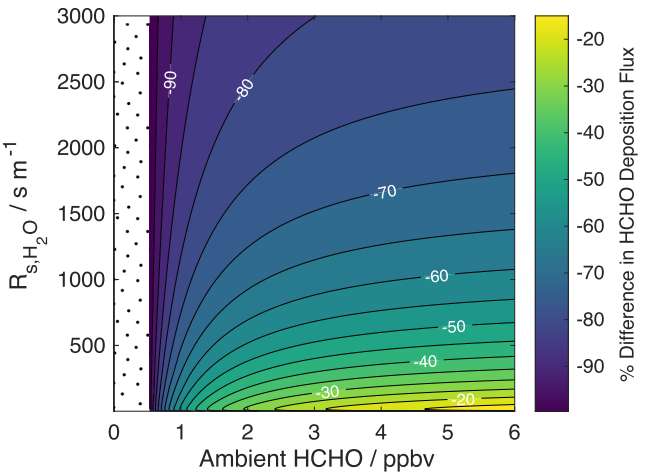

Figure 5. Percent difference in the HCHO deposition flux when using f_0 = 0 and C_i = 0.52 ppbv (HCHO CP at 30 °C) relative to f_0 = 1 and C_i = 0 ppbv. No comparison is made in the dotted region since using f_0 = 0 and C_i = 0.52 ppbv predicts an emission flux.

Given that the HCHO deposition fluxes calculated using experimental recommendations weaken the deposition sink, it is useful to compare the deposition sink against two other sinks of HCHO: photolysis and loss by OH (loss by NO_3 is assumed negligible). A lower predicted deposition flux of HCHO when using f_0 = 0 with nonzero HCHO CP has the effect of increasing the fractional contribution of photolysis and OH as HCHO loss processes. Given that these loss pathways are a source of HO_2,[9] our results suggest that this would have the effect of increasing the oxidative capacity of the atmosphere, in particular in the vicinity of the canopy. While dependent on various factors (e.g., leaf area index, boundary layer height, $R_{c,HCHO}$, etc.), f_0 = 0 with nonzero HCHO CP would increase HO_2 from the other HCHO loss pathways by a few percent.

A 1-D box model, the FORest Canopy Atmosphere Transport model (FORCAsT; see the Supporting Information),[50,61] was also used to check how the dry deposition sink compares against the other major loss processes of HCHO in a forest canopy. Figure 6 shows the percent contribution of dry deposition, photolysis, and reaction with OH to the overall HCHO sink strength within the canopy (6−22.5 m) as a function of ambient HCHO volume mixing ratio (0−1 ppbv) at 30 °C. Reaction with OH is a minor HCHO sink within the canopy, and the two major HCHO sinks are photolysis and dry deposition. At the HCHO CP (0.52 ppbv), there is no contribution of HCHO dry deposition to the total sink. As the ambient HCHO rises above the CP, dry deposition becomes the dominant sink at and above 0.65 ppbv ambient HCHO. This result indicates that the dry deposition contribution to the overall sink strength is very sensitive to HCHO mixing ratios within 0.1 ppbv of the HCHO CP. While the experimentally determined HCHO CP and leaf resistance results have reduced the overall HCHO dry deposition sink strength relative to literature parametrizations, HCHO dry deposition is still expected to be the dominant HCHO sink in the canopy for typical ambient HCHO mixing ratios greater than 1 ppbv.

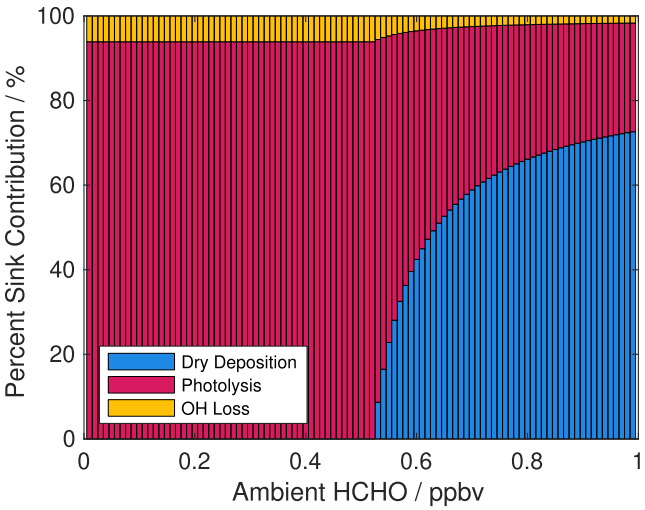

Figure 6. Percent contribution of dry deposition, photolysis, and reaction with OH to the total HCHO sink budget as a function of HCHO mixing ratio when using f_0 = 0 and C_i = 0.52 ppbv (HCHO CP at 30 °C). Each sink is integrated over the canopy region in the FORCAsT model at the University of Michigan Biological Station site.

4. CONCLUSIONS

Leaf-level measurements of HCHO foliar exchange performed under a variety of controlled laboratory conditions provided the first temperature-dependent parametrization for the

https://doi.org/10.1021/acsearthspacechem.3c00325
ACS Earth Space Chem. 2024, 8, 723−733

HCHO CP and a statistically robust data set to assess the performance of commonly used model frameworks for HCHO dry deposition. An exponential temperature dependence was observed for the HCHO CP from 22 to 35 °C with a mean range of 0.3−0.9 ppbv HCHO. Moreover, the CP was statistically shown to be independent of both humidity (40−70%) and a deciduous (*Q. rubra*) versus evergreen (*C.* × *leylandii*) tree species. The results indicate that trees are not likely a primary source of HCHO as daytime mixing ratios in forests are typically larger than 1 ppbv HCHO.

The HCHO leaf resistance and exchange velocities were shown to be controlled primarily by the stomata, which accounted for at least 85% of the HCHO total foliar surface resistance ($R_{c,HCHO}$) even at a nighttime H_2O stomatal resistance (R_{s,H_2O}) of 3000 s m^{-1}. Furthermore, it is recommended that atmospheric chemistry models utilize f_0 = 0 for HCHO as well as incorporate the lab-based CP temperature parametrization. Updating models with these parametrizations results in upward of a 50% reduction in daytime HCHO deposition fluxes. However, dry deposition is still the major sink of HCHO within forest canopies, and a weaker HCHO deposition flux increases atmospheric oxidation given that HO_2 produced from the other HCHO loss pathways (i.e., photolysis and OH) is increased by a few percent.

Overall, the results of this study indicate that HCHO exchange has a larger foliar resistance than currently predicted, which motivates further laboratory-based OVOC bidirectional exchange experiments for the accurate prediction of OVOC sources and sinks in forests. Further experiments should also investigate the impact of tree age (young vs mature) and several tree species on HCHO CP and exchange velocities to assess the applicability and robustness of this study. Additionally, these results suggest that the missing positive flux of HCHO identified in forest canopies and elsewhere is not attributable to direct HCHO emission from foliage but rather to some other process.

■ ASSOCIATED CONTENT

Supporting Information

The Supporting Information is available free of charge at https://pubs.acs.org/doi/10.1021/acsearthspacechem.3c00325.

Description of ANOVA tests, description of FORCAsT model, Figure S1, *Quercus rubra* range map, Figure S2, blank cuvette experiment, Figure S3, $R_{c,HCHO}$ for R_{s,H_2O}> 3000 s m^{-1}, Figure S4, $R_{meso,HCHO}$ and $R_{stom,HCHO}$ for g_{s,H_2O}> 15 mmol m^{-2} s^{-1}, Table S1, HCHO lights on experimental data, Table S2, HCHO lights off experimental data, Table S3, $R_{b,HCHO}$ experiments, Table S4, R_{b,H_2O} experiments, and Table S5, statistical test *p* values (Levene, Shapiro-Wilk, ANOVA, TukeyHSD) (PDF)

■ AUTHOR INFORMATION

Corresponding Author

Frank N. Keutsch − *Department of Chemistry and Chemical Biology, Harvard University, Cambridge, Massachusetts 02138, United States; Harvard John A. Paulson School of Engineering and Applied Sciences and Department of Earth and Planetary Sciences, Harvard University, Cambridge, Massachusetts 02138, United States;* orcid.org/0000-0002-1442-6200; Email: keutsch@seas.harvard.edu

Authors

Joshua D. Shutter − *Department of Chemistry and Chemical Biology, Harvard University, Cambridge, Massachusetts 02138, United States;* Present Address: Department of Soil, Water, and Climate, University of Minnesota, St. Paul, Minnesota 55108

Joshua L. Cox − *Department of Chemistry and Chemical Biology, Harvard University, Cambridge, Massachusetts 02138, United States*

Complete contact information is available at: https://pubs.acs.org/10.1021/acsearthspacechem.3c00325

Author Contributions

⊥J.D.S. and J.L.C. contributed equally to the project and therefore are co-first authors. J.D.S. and J.L.C. conceived and designed the study, carried out laboratory experiments, analyzed the data, and interpreted results. F.N.K. provided supervision and financial support for the project. J.D.S. and J.L.C. prepared and wrote the manuscript in consultation with F.N.K.

Funding

This material is based upon work supported by the National Science Foundation Graduate Research Fellowship under Grant No. DGE-1745303 for both J.D.S. and J.L.C.

Notes

The authors declare no competing financial interest.

■ ACKNOWLEDGMENTS

The authors thank Dr. Alex Guenther and Dr. Sanjeevi Nagalingam for the design of the leaf cuvette setup and for helpful discussions. We also acknowledge Dr. Allison Steiner and Dr. Dandan Wei for help on running the FORCAsT model, and Janet Sherwood of the Harvard OEB Greenhouse for providing guidance and assistance on plant care. Additionally, we acknowledge Dr. Kirk Ullmann and Dr. Samuel Hall for photolysis frequencies obtained during the PROPHET-AMOS field campaign. We further acknowledge Margaux Winter and Yasmeen Fakhro of Harvard College for assisting on the project, Erik Mallory of J.J. Wilbur and Co. for the zero-air generator, and the CCB Facilities team for laboratory and building support.

■ REFERENCES

(1) Heald, C. L.; Kroll, J. H. The Fuel of Atmospheric Chemistry: Toward a Complete Description of Reactive Organic Carbon. *Sci. Adv.* **2020**, *6* (6), No. eaay8967.

(2) Guenther, A. B.; Jiang, X.; Heald, C. L.; Sakulyanontvittaya, T.; Duhl, T.; Emmons, L. K.; Wang, X. The Model of Emissions of Gases and Aerosols from Nature Version 2.1 (MEGAN2.1): An Extended and Updated Framework for Modeling Biogenic Emissions. *Geosci. Model Dev.* **2012**, *5* (6), 1471−1492.

(3) Nguyen, T. B.; Crounse, J. D.; Teng, A. P.; St. Clair, J. M.; Paulot, F.; Wolfe, G. M.; Wennberg, P. O. Rapid Deposition of Oxidized Biogenic Compounds to a Temperate Forest. *Proc. Natl. Acad. Sci. U. S. A.* **2015**, *112* (5), No. E392−E401.

(4) Knote, C.; Hodzic, A.; Jimenez, J. L. The Effect of Dry and Wet Deposition of Condensable Vapors on Secondary Organic Aerosols Concentrations over the Continental US. *Atmos. Chem. Phys.* **2015**, *15* (1), 1−18.

(5) Farmer, D. K.; Riches, M. Measuring Biosphere−Atmosphere Exchange of Short-Lived Climate Forcers and Their Precursors. *Acc. Chem. Res.* **2020**, *53* (8), 1427−1435.
(6) Karl, T.; Harley, P.; Emmons, L.; Thornton, B.; Guenther, A.; Basu, C.; Turnipseed, A.; Jardine, K. Efficient Atmospheric Cleansing of Oxidized Organic Trace Gases by Vegetation. *Science* **2010**, *330* (6005), 816−819.
(7) Zhou, P.; Ganzeveld, L.; Taipale, D.; Rannik, Ü.; Rantala, P.; Rissanen, M. P.; Chen, D.; Boy, M. Boreal Forest BVOC Exchange: Emissions versus in-Canopy Sinks. *Atmos. Chem. Phys.* **2017**, *17* (23), 14309−14332.
(8) Klemm, O.; Held, A.; Forkel, R.; Gasche, R.; Kanter, H.-J.; Rappenglück, B.; Steinbrecher, R.; Müller, K.; Plewka, A.; Cojocariu, C.; Kreuzwieser, J.; Valverde-Canossa, J.; Schuster, G.; Moortgat, G. K.; Graus, M.; Hansel, A. Experiments on Forest/Atmosphere Exchange: Climatology and Fluxes during Two Summer Campaigns in NE Bavaria. *Atmos. Environ.* **2006**, *40*, 3−20.
(9) Heikes, B.; Snow, J.; Egli, P.; O'Sullivan, D.; Crawford, J.; Olson, J.; Chen, G.; Davis, D.; Blake, N.; Blake, D. Formaldehyde over the Central Pacific during PEM-Tropics B. *J. Geophys. Res.* **2001**, *106* (D23), 32717−32731.
(10) Millet, D. B.; Jacob, D. J.; Turquety, S.; Hudman, R. C.; Wu, S.; Fried, A.; Walega, J.; Heikes, B. G.; Blake, D. R.; Singh, H. B.; Anderson, B. E.; Clarke, A. D. Formaldehyde Distribution over North America: Implications for Satellite Retrievals of Formaldehyde Columns and Isoprene Emission, *J. Geophys. Res. Atmos.* **2006**, *111* D24, D24S02.
(11) Choi, W.; Faloona, I. C.; Bouvier-Brown, N. C.; McKay, M.; Goldstein, A. H.; Mao, J.; Brune, W. H.; LaFranchi, B. W.; Cohen, R. C.; Wolfe, G. M.; Thornton, J. A.; Sonnenfroh, D. M.; Millet, D. B. Observations of Elevated Formaldehyde over a Forest Canopy Suggest Missing Sources from Rapid Oxidation of Arboreal Hydrocarbons. *Atmos. Chem. Phys.* **2010**, *10* (18), 8761−8781.
(12) Chan Miller, C.; Jacob, D. J.; Marais, E. A.; Yu, K.; Travis, K. R.; Kim, P. S.; Fisher, J. A.; Zhu, L.; Wolfe, G. M.; Hanisco, T. F.; Keutsch, F. N.; Kaiser, J.; Min, K.-E.; Brown, S. S.; Washenfelder, R. A.; González Abad, G.; Chance, K. Glyoxal Yield from Isoprene Oxidation and Relation to Formaldehyde: Chemical Mechanism, Constraints from SENEX Aircraft Observations, and Interpretation of OMI Satellite Data. *Atmos. Chem. Phys.* **2017**, *17* (14), 8725−8738.
(13) Zhu, L.; Mickley, L. J.; Jacob, D. J.; Marais, E. A.; Sheng, J.; Hu, L.; Abad, G. G.; Chance, K. Long-term (2005−2014) Trends in Formaldehyde (HCHO) Columns Across North America as Seen by the OMI Satellite Instrument: Evidence of Changing Emissions of Volatile Organic Compounds. *Geophys. Res. Lett.* **2017**, *44* (13), 7079−7086.
(14) Wolfe, G. M.; Kaiser, J.; Hanisco, T. F.; Keutsch, F. N.; de Gouw, J. A.; Gilman, J. B.; Graus, M.; Hatch, C. D.; Holloway, J.; Horowitz, L. W.; Lee, B. H.; Lerner, B. M.; Lopez-Hilifiker, F.; Mao, J.; Marvin, M. R.; Peischl, J.; Pollack, I. B.; Roberts, J. M.; Ryerson, T. B.; Thornton, J. A.; Veres, P. R.; Warneke, C. Formaldehyde Production from Isoprene Oxidation Across NO_x Regimes. *Atmos. Chem. Phys.* **2016**, *16* (4), 2597−2610.
(15) Sivakumaran, V.; Hölscher, D.; Dillon, T. J.; Crowley, J. N. Reaction Between OH and HCHO: Temperature Dependent Rate Coefficients (202−399 K) and Product Pathways (298 K). *Phys. Chem. Chem. Phys.* **2003**, *5* (21), 4821−4827.
(16) Lin, Y. C.; Schwab, J. J.; Demerjian, K. L.; Bae, M.-S.; Chen, W.-N.; Sun, Y.; Zhang, Q.; Hung, H.-M.; Perry, J. Summertime Formaldehyde Observations in New York City: Ambient Levels, Sources and Its Contribution to HO_x Radicals, *J. Geophys. Res. Atmos.* **2012**, *117* D8, D08305.
(17) Kesselmeier, J.; Bode, K.; Hofmann, U.; Müller, H.; Schäfer, L.; Wolf, A.; Ciccioli, P.; Brancaleoni, E.; Cecinato, A.; Frattoni, M.; Foster, P.; Ferrari, C.; Jacob, V.; Fugit, J. L.; Dutaur, L.; Simon, V.; Torres, L. Emission of Short Chained Organic Acids, Aldehydes and Monoterpenes from *Quercus Ilex* L. and *Pinus Pinea* L. in Relation to Physiological Activities, Carbon Budget and Emission Algorithms. *Atmos. Environ.* **1997**, *31*, 119−133.
(18) Kesselmeier, J. Exchange of Short-Chain Oxygenated Volatile Organic Compounds (VOCs) between Plants and the Atmosphere: A Compilation of Field and Laboratory Studies. *J. Atmos. Chem.* **2001**, *39* (3), 219−233.
(19) Kreuzwieser, J.; Cojocariu, C.; Jüssen, V.; Rennenberg, H. Elevated Atmospheric CO_2 Causes Seasonal Changes in Carbonyl Emissions from *Quercus ilex*. *New Phytol.* **2002**, *154* (2), 327−333.
(20) Cojocariu, C.; Kreuzwieser, J.; Rennenberg, H. Correlation of Short-Chained Carbonyls Emitted from *Picea abies* with Physiological and Environmental Parameters. *New Phytol.* **2004**, *162* (3), 717−727.
(21) Rottenberger, S.; Kuhn, U.; Wolf, A.; Schebeske, G.; Oliva, S. T.; Tavares, T. M.; Kesselmeier, J. Exchange of Short-Chain Aldehydes Between Amazonian Vegetation and the Atmosphere. *Ecol. Appl.* **2004**, *14* (sp4), 247−262.
(22) Kreuzwieser, J.; Rennenberg, H.; Steinbrecher, R. Impact of Short-Term and Long-Term Elevated CO_2 on Emission of Carbonyls from Adult *Quercus petraea* and *Carpinus betulus* Trees. *Environ. Pollut.* **2006**, *142* (2), 246−253.
(23) Seco, R.; Peñuelas, J.; Filella, I. Formaldehyde Emission and Uptake by Mediterranean Trees *Quercus ilex* and *Pinus halepensis*. *Atmos. Environ.* **2008**, *42* (34), 7907−7914.
(24) Brasseur, G. P.; Jacob, D. J. *Modeling of Atmospheric Chemistry*; Cambridge University Press: Cambridge, 2017.
(25) Shutter, J.; Keutsch, F. *Biosphere-Atmosphere Interactions*; ACS In Focus; American Chemical Society, 2021.
(26) DiGangi, J. P.; Boyle, E. S.; Karl, T.; Harley, P.; Turnipseed, A.; Kim, S.; Cantrell, C.; Maudlin III, R. L.; Zheng, W.; Flocke, F.; Hall, S. R.; Ullmann, K.; Nakashima, Y.; Paul, J. B.; Wolfe, G. M.; Desai, A. R.; Kajii, Y.; Guenther, A.; Keutsch, F. N. First Direct Measurements of Formaldehyde Flux via Eddy Covariance: Implications for Missing in-Canopy Formaldehyde Sources. *Atmos. Chem. Phys.* **2011**, *11* (20), 10565−10578.
(27) Kaiser, J.; Wolfe, G. M.; Bohn, B.; Broch, S.; Fuchs, H.; Ganzeveld, L. N.; Gomm, S.; Häseler, R.; Hofzumahaus, A.; Holland, F.; Jäger, J.; Li, X.; Lohse, I.; Lu, K.; Prévôt, A. S. H.; Rohrer, F.; Wegener, R.; Wolf, R.; Mentel, T. F.; Kiendler-Scharr, A.; Wahner, A.; Keutsch, F. N. Evidence for an Unidentified Non-Photochemical Ground-Level Source of Formaldehyde in the Po Valley with Potential Implications for Ozone Production. *Atmos. Chem. Phys.* **2015**, *15* (3), 1289−1298.
(28) Juráň, S.; Pallozzi, E.; Guidolotti, G.; Fares, S.; Šigut, L.; Calfapietra, C.; Alivernini, A.; Savi, F.; Večeřová, K.; Křůmal, K.; Večeřa, Z.; Urban, O. Fluxes of Biogenic Volatile Organic Compounds above Temperate Norway Spruce Forest of the Czech Republic. *Agric. For. Meteorol.* **2017**, *232*, 500−513.
(29) Wesely, M. L. Parameterization of Surface Resistances to Gaseous Dry Deposition in Regional-Scale Numerical Models. *Atmos. Environ.* **1989**, *23* (6), 1293−1304.
(30) Millet, D. B.; Alwe, H. D.; Chen, X.; Deventer, M. J.; Griffis, T. J.; Holzinger, R.; Bertman, S. B.; Rickly, P. S.; Stevens, P. S.; Léonardis, T.; Locoge, N.; Dusanter, S.; Tyndall, G. S.; Alvarez, S. L.; Erickson, M. H.; Flynn, J. H. Bidirectional Ecosystem−Atmosphere Fluxes of Volatile Organic Compounds Across the Mass Spectrum: How Many Matter? *ACS Earth Space Chem.* **2018**, *2* (8), 764−777.
(31) Harley, P.; Eller, A.; Guenther, A.; Monson, R. K. Observations and Models of Emissions of Volatile Terpenoid Compounds from Needles of Ponderosa Pine Trees Growing in Situ: Control by Light, Temperature and Stomatal Conductance. *Oecologia* **2014**, *176* (1), 35−55.
(32) Nagalingam, S.; Seco, R.; Kim, S.; Guenther, A. Heat Stress Strongly Induces Monoterpene Emissions in Some Plants with Specialized Terpenoid Storage Structures. *Agric. For. Meteorol.* **2023**, *333*, 109400.
(33) Pape, L.; Ammann, C.; Nyfeler-Brunner, A.; Spirig, C.; Hens, K.; Meixner, F. X. An Automated Dynamic Chamber System for Surface Exchange Measurement of Non-Reactive and Reactive Trace Gases of Grassland Ecosystems. *Biogeosciences* **2009**, *6* (3), 405−429.
(34) Hottle, J. R.; Huisman, A. J.; DiGangi, J. P.; Kammrath, A.; Galloway, M. M.; Coens, K. L.; Keutsch, F. N. A Laser Induced

https://doi.org/10.1021/acsearthspacechem.3c00325
ACS Earth Space Chem. 2024, 8, 723−733

Fluorescence-Based Instrument for In-Situ Measurements of Atmospheric Formaldehyde. *Environ. Sci. Technol.* **2009**, *43* (3), 790−795.
(35) Cazorla, M.; Wolfe, G. M.; Bailey, S. A.; Swanson, A. K.; Arkinson, H. L.; Hanisco, T. F. A New Airborne Laser-Induced Fluorescence Instrument for in Situ Detection of Formaldehyde throughout the Troposphere and Lower Stratosphere. *Atmos. Meas. Tech.* **2015**, *8* (2), 541−552.
(36) Shutter, J. D.; Allen, N. T.; Hanisco, T. F.; Wolfe, G. M.; St. Clair, J. M.; Keutsch, F. N. A New Laser-Based and Ultra-Portable Gas Sensor for Indoor and Outdoor Formaldehyde (HCHO) Monitoring. *Atmos. Meas. Tech.* **2019**, *12* (11), 6079−6089.
(37) DiGangi, J. P.; Henry, S. B.; Kammrath, A.; Boyle, E. S.; Kaser, L.; Schnitzhofer, R.; Graus, M.; Turnipseed, A.; Park, J.-H.; Weber, R. J.; Hornbrook, R. S.; Cantrell, C. A.; Maudlin III, R. L.; Kim, S.; Nakashima, Y.; Wolfe, G. M.; Kajii, Y.; Apel, E. C.; Goldstein, A. H.; Guenther, A.; Karl, T.; Hansel, A.; Keutsch, F. N. Observations of Glyoxal and Formaldehyde as Metrics for the Anthropogenic Impact on Rural Photochemistry. *Atmos. Chem. Phys.* **2012**, *12* (20), 9529−9543.
(38) Niinemets, Ü.; Kuhn, U.; Harley, P. C.; Staudt, M.; Arneth, A.; Cescatti, A.; Ciccioli, P.; Copolovici, L.; Geron, C.; Guenther, A.; Kesselmeier, J.; Lerdau, M. T.; Monson, R. K.; Peñuelas, J. Estimations of Isoprenoid Emission Capacity from Enclosure Studies: Measurements, Data Processing, Quality and Standardized Measurement Protocols. *Biogeosciences* **2011**, *8* (8), 2209−2246.
(39) Breuninger, C.; Oswald, R.; Kesselmeier, J.; Meixner, F. X. The Dynamic Chamber Method: Trace Gas Exchange Fluxes (NO, NO_2, O_3) between Plants and the Atmosphere in the Laboratory and in the Field. *Atmos. Meas. Tech.* **2012**, *5* (5), 955−989.
(40) York, D.; Evensen, N. M.; Martínez, M. L.; De Basabe Delgado, J. Unified Equations for the Slope, Intercept, and Standard Errors of the Best Straight Line. *Am. J. Phys.* **2004**, *72* (3), 367−375.
(41) Easlon, H. M.; Bloom, A. J. Easy Leaf Area: Automated Digital Image Analysis for Rapid and Accurate Measurement of Leaf Area. *Appl. Plant Sci.* **2014**, *2* (7), 1400033.
(42) Niinemets, Ü.; Fares, S.; Harley, P.; Jardine, K. J. Bidirectional Exchange of Biogenic Volatiles with Vegetation: Emission Sources, Reactions, Breakdown and Deposition: Bidirectional BVOC Exchange. *Plant Cell Environ.* **2014**, *37* (8), 1790−1809.
(43) Sun, S.; Moravek, A.; Trebs, I.; Kesselmeier, J.; Sörgel, M. Investigation of the Influence of Liquid Surface Films on O_3 and PAN Deposition to Plant Leaves Coated with Organic/Inorganic Solution. *J. Geophys. Res. Atmos.* **2016**, *121* (23), 14,239−14,256.
(44) Delaria, E. R.; Vieira, M.; Cremieux, J.; Cohen, R. C. Measurements of NO and NO_2 Exchange between the Atmosphere and *Quercus agrifolia*. *Atmos. Chem. Phys.* **2018**, *18* (19), 14161−14173.
(45) CarstenRobens. MATLAB Central File Exchange: Monte Carlo Error Propagation, 2016. https://www.mathworks.com/matlabcentral/fileexchange/57672-monte-carlo-error-propagation (accessed 2020−04−01).
(46) von Caemmerer, S.; Farquhar, G. D. Some Relationships between the Biochemistry of Photosynthesis and the Gas Exchange of Leaves. *Planta* **1981**, *153* (4), 376−387.
(47) Parkinson, K. J. A Simple Method for Determining the Boundary Layer Resistance in Leaf Cuvettes. *Plant Cell Environ.* **1985**, *8* (3), 223−226.
(48) Karl, T.; Harley, P.; Guenther, A.; Rasmussen, R.; Baker, B.; Jardine, K.; Nemitz, E. The Bi-Directional Exchange of Oxygenated VOCs between a Loblolly Pine (*Pinus taeda*) Plantation and the Atmosphere. *Atmos. Chem. Phys.* **2005**, *5*, 3015−3031.
(49) Galloway, M. M.; DiGangi, J. P.; Hottle, J. R.; Huisman, A. J.; Mielke, L. H.; Alaghmand, M.; Shepson, P. B.; Weremijewicz, J.; Klavon, H.; McNeal, F. M.; Carroll, M. A.; Griffith, S.; Hansen, R. F.; Dusanter, S.; Stevens, P. S.; Bertman, S. B.; Keutsch, F. N. Observations and Modeling of Formaldehyde at the PROPHET Mixed Hardwood Forest Site in 2008. *Atmos. Environ.* **2012**, *49*, 403−410.
(50) Wei, D.; Alwe, H. D.; Millet, D. B.; Bottorff, B.; Lew, M.; Stevens, P. S.; Shutter, J. D.; Cox, J. L.; Keutsch, F. N.; Shi, Q.; Kavassalis, S. C.; Murphy, J. G.; Vasquez, K. T.; Allen, H. M.; Praske, E.; Crounse, J. D.; Wennberg, P. O.; Shepson, P. B.; Bui, A. A. T.; Wallace, H. W.; Griffin, R. J.; May, N. W.; Connor, M.; Slade, J. H.; Pratt, K. A.; Wood, E. C.; Rollings, M.; Deming, B. L.; Anderson, D. C.; Steiner, A. L. FORest Canopy Atmosphere Transfer (FORCAsT) 2.0: Model Updates and Evaluation with Observations at a Mixed Forest Site. *Geosci. Model Dev.* **2021**, *14* (10), 6309−6329.
(51) Jardine, K. J.; Jardine, A. B.; Souza, V. F.; Carneiro, V.; Ceron, J. V.; Gimenez, B. O.; Soares, C. P.; Durgante, F. M.; Higuchi, N.; Manzi, A. O.; Gonçalves, J. F. C.; Garcia, S.; Martin, S. T.; Zorzanelli, R. F.; Piva, L. R.; Chambers, J. Q. Methanol and Isoprene Emissions from the Fast Growing Tropical Pioneer Species *Vismia guianensis* (Aubl.) Pers. (Hypericaceae) in the Central Amazon Forest. *Atmos. Chem. Phys.* **2016**, *16* (10), 6441−6452.
(52) Inomata, S.; Tanimoto, H.; Kameyama, S.; Tsunogai, U.; Irie, H.; Kanaya, Y.; Wang, Z. Technical Note: Determination of Formaldehyde Mixing Ratios in Air with PTR-MS: Laboratory Experiments and Field Measurements. *Atmos. Chem. Phys.* **2008**, *8* (2), 273−284.
(53) Vlasenko, A.; Macdonald, A. M.; Sjostedt, S. J.; Abbatt, J. P. D. Formaldehyde Measurements by Proton transfer Reaction − Mass Spectrometry (PTR-MS): Correction for Humidity Effects. *Atmos. Meas. Tech.* **2010**, *3* (4), 1055−1062.
(54) Warneke, C.; Veres, P.; Holloway, J. S.; Stutz, J.; Tsai, C.; Alvarez, S.; Rappenglueck, B.; Fehsenfeld, F. C.; Graus, M.; Gilman, J. B.; de Gouw, J. A. Airborne Formaldehyde Measurements Using PTR-MS: Calibration, Humidity Dependence, Inter-Comparison and Initial Results. *Atmos. Meas. Tech.* **2011**, *4* (10), 2345−2358.
(55) Seco, R.; Peñuelas, J.; Filella, I. Short-Chain Oxygenated VOCs: Emission and Uptake by Plants and Atmospheric Sources, Sinks, and Concentrations. *Atmos. Environ.* **2007**, *41* (12), 2477−2499.
(56) Wisthaler, A.; Apel, E. C.; Bossmeyer, J.; Hansel, A.; Junkermann, W.; Koppmann, R.; Meier, R.; Müller, K.; Solomon, S. J.; Steinbrecher, R.; Tillmann, R.; Brauers, T. Technical Note: Intercomparison of Formaldehyde Measurements at the Atmosphere Simulation Chamber SAPHIR. *Atmos. Chem. Phys.* **2008**, *8* (8), 2189−2200.
(57) Wiens, T. MATLAB Central File Exchange: Linear Regression with Errors in X and Y, 2010. https://www.mathworks.com/matlabcentral/fileexchange/26586-linear-regression-with-errors-in-x-and-y (accessed 2020−04−06).
(58) Ipek. MATLAB Central File Exchange: Normality Test Package, 2018. https://www.mathworks.com/matlabcentral/fileexchange/60147-normality-test-package (accessed 2020−04−05).
(59) Komarov, O.. MATLAB Central File Exchange: Heteroskedasticity Test, 2009. https://www.mathworks.com/matlabcentral/fileexchange/24722-heteroskedasticity-test (accessed 2020−04−05).
(60) Sander, R. Compilation of Henry's Law Constants (Version 4.0) for Water as Solvent. *Atmos. Chem. Phys.* **2015**, *15* (8), 4399−4981.
(61) Ashworth, K.; Chung, S. H.; Griffin, R. J.; Chen, J.; Forkel, R.; Bryan, A. M.; Steiner, A. L. FORest Canopy Atmosphere Transfer (FORCAsT) 1.0: a 1-D Model of Biosphere−Atmosphere Chemical Exchange. *Geosci. Model Dev.* **2015**, *8* (11), 3765−3784.

https://doi.org/10.1021/acsearthspacechem.3c00325
ACS Earth Space Chem. 2024, 8, 723−733